Functional Assessment of Inner and Outer Macular Layers in Idiopathic Epiretinal Membrane

Vincenzo Parisi,[1,2] Lucia Ziccardi,[1,3] Carmen Dell'Aquila,[1] Lucilla Barbano,[1] Mattia D'Andrea,[4] Sara Giammaria,[1] Guido Ripandelli,[1] Luca Placentino,[1] Roberto dell'Omo,[3] and Tommaso Rossi[1]

[1]IRCCS–Fondazione Bietti, Rome, Italy
[2]Departmental Faculty of Medicine, UniCamillus-Saint Camillus International University of Health Sciences, Rome, Italy
[3]Department of Medicine and Health Sciences "V. Tiberio," University of Molise, Campobasso, Italy
[4]Department of Sense Organs, Faculty of Medicine and Dentistry, Sapienza University of Rome, Rome, Italy

Correspondence: Lucia Ziccardi, IRCCS–Fondazione Bietti, Via Livenza 1, Rome 00198, Italy; lucia.ziccardi@fondazionebietti.it.

Received: August 8, 2025
Accepted: November 8, 2025
Published: December 9, 2025

Citation: Parisi V, Ziccardi L, Dell'Aquila C, et al. Functional assessment of inner and outer macular layers in idiopathic epiretinal membrane. *Invest Ophthalmol Vis Sci.* 2025;66(15):29. https://doi.org/10.1167/iovs.66.15.29

Purpose. To evaluate the function of macular ganglion cells and nerve fibers in idiopathic epiretinal membrane (ERM), using multifocal photopic negative response (mfPhNR) recordings, to evaluate the function of macular photoreceptors and bipolar cells using multifocal electroretinogram (mfERG) recordings, and to investigate the correlation between the function of those different retinal elements with the changes of visual acuity and central retinal thickness (CRT).

Methods. The study included 16 eyes of 16 patients (mean age, 67.25 ± 6.38 years) with stage 4 ERM (16 eyes) and 28 age-matched controls (mean age, 68.03 ± 7.18 years). Main outcome measures included best-corrected visual acuity (BCVA), CRT, mfPhNR, and mfERG.

Results. ERM eyes showed significantly reduced ($P < 0.01$) mfPhNR response amplitude densities (RADs) in all examined circular areas enclosed between 0° to 10° and 10° to 25° and in superior, nasal, inferior, and temporal sectors within 5° to 20° compared to controls. There was no significant correlation between abnormal mfPhNR RADs within the central 0° to 10° and BCVA or CRT. The mfERG RADs in the central 0° to 10° were significantly reduced and linearly correlated to BCVA reduction ($P < 0.01$) but not to mfPhNR RADs and CRT.

Conclusions. Our data suggest an unrelated dysfunction of both inner and outer macular layers, occurring in the central 0° to 10°, and an exclusive inner macular dysfunction in the more peripheral areas (10°–25°). The reduction of BCVA correlated only to the central outer macular dysfunction.

Keywords: epiretinal membranes, electroretinogram, retinal function, macula, SD-OCT

Idiopathic epiretinal membranes (ERMs) may form on the surface of the internal limiting membrane (ILM) after incomplete detachment of the posterior vitreous.[1] This tissue is composed of cells with contractile capability, causing profound morphofunctional alterations in both the inner and outer retina layers with loss of physiological foveal depression and increased central retinal thickness (CRT).[2,3] In the clinical settings, ERMs leading to a visual dysfunction[4–6] can be detectable in vivo by optical coherence tomography (OCT)[7–10] and classified as stages 1 to 4, based on ultrastructural findings, according to Govetto et al.[11]

In ERM eyes, the use of focal electroretinogram (FERG)[12] and multifocal electroretinogram (mfERG)[13] has revealed a dysfunction of preganglionic elements located in the more central macular areas.[14–16] By contrast, pattern electroretinogram (PERG) was found to be abnormal in the whole central 9°, without the possibility of identifying selective impairment of localized ganglionic elements.[14] The new paradigm of the multifocal photopic negative response (mfPhNR) investigates the localized functional responses of the inner retinal elements from regional macular areas.[17] Ganglion cell dysfunction in localized retinal areas has already been studied by using mfPhNR in patients with optic neuritis in multiple sclerosis,[17,18] as well as in patients with open-angle glaucoma.[19] The purpose of the present study was to evaluate the function of the inner (by mfPhNR) and outer (by mfERG) retinal layers of localized macular regions in ERM eyes and to investigate the correlation between the inner retinal function (macular ganglion cells and nerve fibers) and outer retina elements (photoreceptors and bipolar cells) and/or the changes of visual acuity and CRT.

Methods

The study adhered to the tenets of the Declaration of Helsinki and received approval by the local Ethics

Committee (Comitato Etico Territoriale Lazio Area 5, IRCCS Istituti Fisioterapici Ospitalieri, Roma, Italy; protocol no. 339/FB/25). Informed consent after full explanation of the procedure was obtained from each enrolled patient.

This retrospective, case–control study drew upon a wide cohort of 82 consecutive eyes presenting with ERMs. Based on the exclusion criteria (see below), 16 eyes from 16 patients (eight men and eight women; mean age, 67.25 ± 6.38 years) with ERM stage 4, according to the ERM staging by Govetto et al.,[11] were selected for the study (16 ERM eyes). All patients underwent electrophysiological study of localized the inner and outer retinal areas within 25° from the fovea by mfPhNR and mfERG recordings, respectively. Because several pathologies may induce changes in mfPhNR and mfERG responses,[20–26] the studied eyes were selected on the basis of the following exclusion criteria: absence of target fixation placed on the monitor screen during the electrophysiological recordings; presence of lens opacity with a severity grade > 1.5 for nuclear, cortical, and posterior subcapsular opacities according to the Age-Related Eye Disease Study (AREDS) System for Classifying Cataracts From Photographs[27]; ocular hypertension or glaucoma, diabetic retinopathy, drusen, or age-related macular degeneration; or history of uveitis and optic neuritis. Also, eyes from patients with systemic diseases such as hypertension, diabetes, connective tissue, or neurological diseases were also excluded. All ERM eyes enrolled were phakic, and the refractive error was between ±1.50 equivalent spherical diopters.

From a wide cohort of consecutive 102 eyes without ERMs, based on the above-mentioned exclusion criteria 28 eyes from 28 age-similar patients (14 men and 14 women; mean age, 68.03 ± 7.18 years) were selected and provided the control data for the study (28 control eyes). All control eyes were phakic, and the refractive error was between ±1.50 spherical equivalent diopters. In ERM and control eyes, best-corrected visual acuity (BCVA), expressed in logMAR values, and CRT, measured using spectral-domain OCT (SD-OCT; Heidelberg Eye Explorer; Heidelberg Engineering, Heidelberg, Germany), were assessed following the methods and criteria for ERM staging suggested by Govetto et al.[11] MfPhNRs and mfERGs were assessed by using the following methods.

mfPhNR and mfERG Recordings

The mfPhNR and mfERG recordings were obtained from ERM and control eyes by using a Diagnosys system (Diagnosys, Lowell, MA, USA), according to our previously published method[17,18,26] following the 2011 International Society for Clinical Electrophysiology of Vision (ISCEV) standards.[28,29] For the mfPhNR recordings, the multifocal stimulus consisted of a circular stimulus of 60 elongated scaled dart pattern "segments" presented on the same monitor screen, with a mean background luminance of 200 cd/m^2 at a viewing distance of 33 cm. Stimulus frequency was 7 Hz. Each "segment" independently alternated between black (0 cd/m^2) and white (400 cd/m^2) according to a maximum length sequence of 12 bits.[17]

For the mfERG, the multifocal stimulus, consisted of 61 scaled hexagons and was displayed on a high-resolution, black-and-white 32-inch liquid-crystal display (LCD) monitor (69 × 38 cm) with a frame rate of 75 Hz. The array of hexagons subtended 50° of visual field (25° radius from the fixation point to edge of display). Each hexagon independently alternated between black (1 cd/m^2) and white (200 cd/m^2) according to a binary maximum length sequence.

In all subjects, mfPhNRs and mfERGs were binocularly recorded after pupil dilation (1% tropicamide) to a diameter of 7 to 8 mm. The cornea was anesthetized with 0.4% benoxinate eye drops. For all recordings, an active Dawson, Trick, and Litzkow bipolar contact electrode, a reference electrode (Ag/AgCl skin electrode placed on the corresponding outer canthi), and a small Ag/AgCl skin ground electrode, placed in center of the forehead, were used. Interelectrode resistance was lower than 3 kOhm. The signal was filtered (bandpass 3–100 Hz) using a Diagnosys Espion system. After automatic rejection of artifacts, the first-order kernel response was considered. In the analysis of the mfPhNRs and mfERGs, averaged response amplitude densities (RADs) were measured in nanoVolt/degree^2 (nV/deg^2) as described in our previous works.[17–19,25,26] As explained in detail in Figures 1, 2, and 3, the mfPhNR and mfERG responses were analyzed by using two different topographies:

1. Ring analysis
2. Early Treatment of Diabetic Retinopathy Study (ETDRS) sector analysis

Statistical Analysis

We assumed a Gaussian distribution of our data. The normal distribution was assessed by using the Kolmogorov–Smirnov test for controls and ERM data. Also, Grubbs' tests did not show outliers for the parameters of each analyzed group. Sample size estimates were obtained from pilot evaluations performed in 10 eyes from 10 patients with ERM and 10 eyes from 10 control subjects other than those included in the current study (unpublished data). The sizing was based on the following mfPhNR ring 1 (R1) RAD values: 24.7 ± 7.6 nV/deg^2 for controls and 15.8 ± 6.8 nV/deg^2 for ERM patients at α = 5% (type 1 error) and power = 80% (β = 20%), giving us at least 12 participants for each group. Descriptive statistics are shown as mean ± SD. Electrophysiological data from controls and ERM patients were compared by using one-way analysis of variance (ANOVA), considering groups as factors. Data for the control 95% lower limit were used to highlight how many ERM eyes showed abnormal mfPhNR and mfERG RAD values. The 95% confidence limits (CLs) were obtained from the control data. One eye of each patient was included in the analysis.

In the whole study population, both linear and nonlinear regression analyses were also used to explore the relationship between mfPhNR and mfERG data in the corresponding rings/areas and sectors. A segmented regression model with breakpoint estimation was also used to analyze mfERG and mfPhNR values yielded by the ring analysis in the control and ERM group. Differences between slopes obtained in the two groups were also computed.

Finally, mfPhNR and mfERG data were correlated with the corresponding values of BCVA and of CRT. Pearson correlation coefficients were computed to assess the strength of these morphofunctional relationships. $P < 0.01$ was considered statistically significant. SPSS Statistics 25 (IBM, Chicago, IL, USA), MedCalc 13.0.4.0 (MedCalc, Mariakerke, Belgium), and R 4.3.1 (R Foundation for Statistical Computing, Vienna, Austria) were used for statistical analysis.

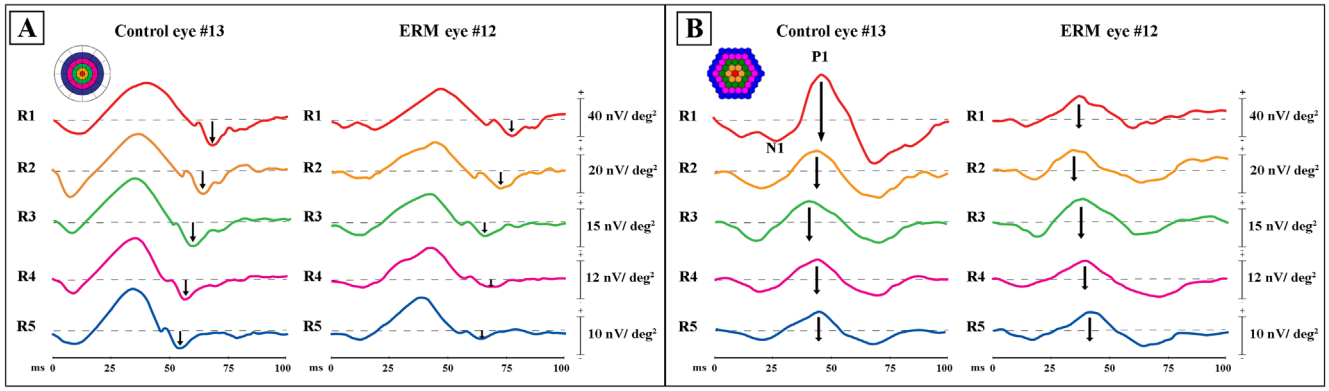

Figure 1. Representative examples of mfPhNR and mfERG averaged traces recorded from one control eye (#13) and one eye with epiretinal membrane (ERM#12) analyzed by ring configuration. (**A**) The mfPhNR RADs were measured (in nV/deg^2) from baseline to trough with implicit times between 50 and 90 ms from the stimulus onset and are indicated by an *arrow* (↓). MfPhNR RADs were obtained from five concentric annular areas (rings) centered on the fovea (R1, central circular area of 5° of radius; R2, annular area enclosed between 5° and10°; R3, annular area enclosed between 10° and 15°; R4, annular area enclosed between 15° and 20°; R5, annular area enclosed between 20° and 25°). In ERM eyes, reduced mfPhNR RADs from all rings were observed with respect to control eyes. (**B**) The mfERG RADs were measured between the N1 and P1 peaks and are indicated by an *arrow* (↕). The mfERG RADs were obtained from five concentric annular areas (rings) centered on the fovea (R1–R5). In ERM eyes, reduced mfERG RADs were observed exclusively in R1 and R2 in comparison to the control eyes.

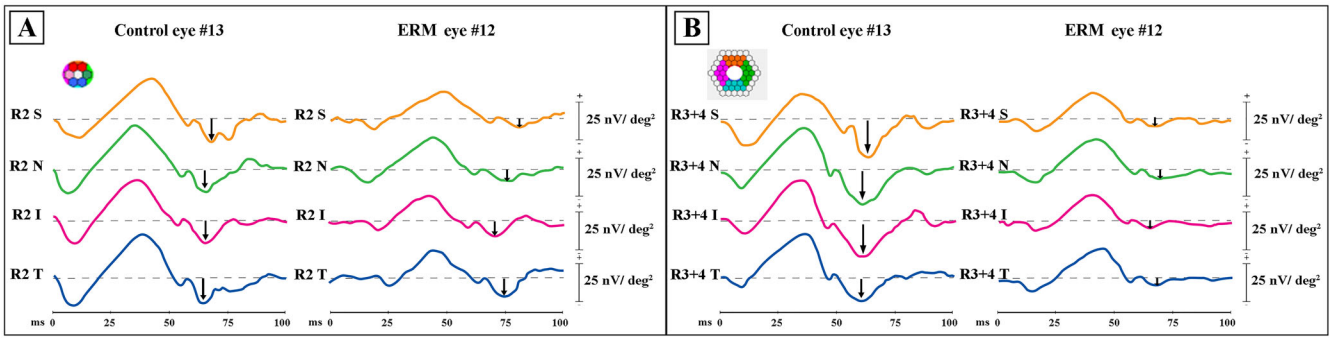

Figure 2. Representative examples of mfPhNR averaged traces recorded from one control eye (#13) and one eye with epiretinal membrane (ERM#12), analyzed by sector configuration. (**A**, **B**) The mfPhNR RADs were measured from baseline to trough with an implicit time between 50 and 90 ms from the stimulus onset and are indicated by an *arrow* (↓). The mfPhNR RADs were obtained on eight sectors following the ETDRS maps: four sectors (S, N, I, T) enclosed between 5° and 10° (R2) (**A**) and four sectors (S, N, I, T) enclosed between 10° and 20° (R3+R4) (**B**). In the ERM eyes, reduced mfPhNR RADs were observed in all sectors with respect to the control eye.

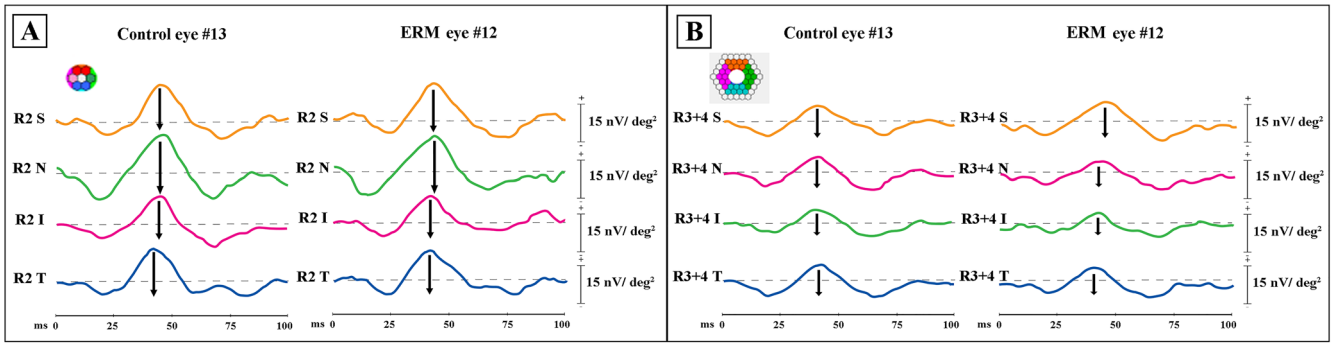

Figure 3. Representative examples of mfERG averaged traces recorded from one control eye (#13) and one eye with epiretinal membrane (ERM#12), analyzed by sector configuration. (**A**, **B**) The mfERG RADs were measured between the N1 and P1 peaks. The mfERG RADs were obtained from eight sectors following the ETDRS maps: four sectors (S, N, I, T) enclosed between 5° and 10° (R2) (**A**) and four sectors (S, N, I, T) enclosed between 10° and 20° (R3+R4) (B). In the ERM eyes, the mfERG RADs observed in all sectors were similar to those of the control eye.

Investigative Ophthalmology & Visual Science

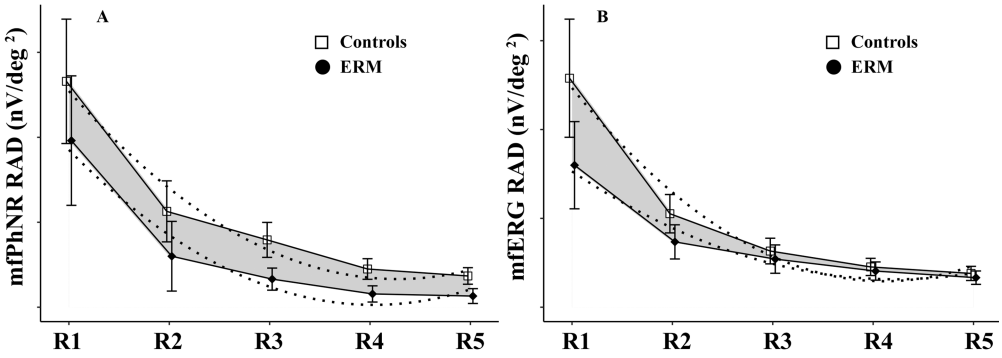

Figure 4. The mfPhNR and mfERG values yielded by the ring analysis (R1–R5) in the control and ERM groups analyzed by a segmented regression model with breakpoint estimation. Differences between slopes were also computed, and the relative statistical analysis is reported in Table 4. *Dashed lines* indicate the polynomial fitting for the mfPhNRs and mfERGs in the control and ERM groups. (**A**) Analysis of the mfPhNR values indicated that differences between the slope of the control eyes and the ERM eyes were constant between R1 and R2 and from R3 to R5. (**B**) Analysis of mfERG values indicated that differences in slope between R1 and R2 and R3 to R5 were not constant; the differences were greater in the first two rings than in R3 to R5.

Results

The values of BCVA, CRT, and mfPhNR and mfERG RADs detected in individual ERM eyes and recorded in rings and ETDRS sectors are reported on Tables 1 and 2. Examples of representative mfPhNR and mfERG responses recorded in one ERM eye (ERM#12) and in one control eye (Control#13) are shown in Figure 1 (ring analysis) and Figures 2 and 3 (sector analysis).

MfPhNR Responses: Ring Analysis

Most ERM eyes showed reduced mfPhNR ring responses (from 62.50% in R1 to 100% in R3 and R4) (Tables 1, 3). On average, in all rings, mfPhNR responses detected in the ERM group were significantly ($P < 0.01$) reduced with respect to controls. The mean values and the relative statistical analyses between control and ERM groups are reported in Table 3. When analyzing mfPhNR values by the segmented regression model with breakpoint estimation in the control and ERM groups, the difference between the slopes of control eyes and ERM eyes was constant between R1 and R2 and from R3 to R5 (−1.694 vs. −1.12632), indicating similar inner retinal dysfunction between the central and the peripheral rings in the ERM group. This finding is shown in Figure 4A and Table 4.

MfPhNR Responses: ETDRS Sector Analysis

Considering individual values, we detected reduced mfPhNR sector responses in most of the eyes of the ERM group,

Table 1. Individual Values of BCVA, CRT, and mfPhNR Detected in Eyes With ERMs

ERM	BCVA (logMAR)	CRT (µm)	Rings mfPhNR RADs (nV/deg²) R1	R2	R3	R4	R5	ETDRS Sectors mfPhNR R2 RADs (nV/deg²) S	N	I	T	ETDRS Sectors mfPhNR R3+R4 RADs (nV/deg²) S	N	I	T
1	0.4	489	31.4	10.2	*3.6*	*1.8*	*1.3*	20.6	*9.4*	*10.3*	17.5	*3.7*	7.0	*1.7*	*2.6*
2	0.3	490	*16.4*	*1.3*	*0.4*	*1.5*	*0.6*	*3*	*6.4*	*3.7*	*1.5*	*0.2*	*2.0*	*1.5*	*1.4*
3	0.5	585	*13.8*	*3.1*	*3.7*	*3.5*	*1.0*	*5.9*	*6.6*	*5.7*	*4.4*	*4.9*	*3.7*	*1.4*	*2.6*
4	0.4	432	*11.1*	*9.7*	*3.8*	*0.1*	*1.6*	17.2	*11.8*	*10.3*	18.7	*4.7*	6.8	6.5	10.2
5	0.2	491	29.4	*5.8*	*4.4*	*1.1*	*0.2*	19.9	19.8	*7.6*	*7.0*	*2.1*	*3.8*	6.2	*2.8*
6	0.5	427	*6.5*	*7.0*	*5.2*	*1.3*	*0.7*	*6.5*	14.6	*6.8*	*11.6*	*2.9*	7.3	*2.3*	*2.1*
7	0.4	534	*17.0*	*2.0*	*2.2*	*1.1*	*2.8*	*6.9*	*5.7*	*8*	*5.5*	*1.5*	*2.9*	*2.8*	*1.8*
8	0.7	487	26.7	*4.6*	*3.1*	*0.9*	*1.0*	*6.2*	*2.2*	*9.9*	*13.2*	*1.5*	*2.4*	*2.3*	*2.6*
9	0.7	645	*16.0*	*2.1*	*1.8*	*0.9*	*1.0*	*5.5*	*1.8*	*6.4*	*6.2*	*1.3*	*3.5*	*2.4*	*1.9*
10	0.5	497	23.9	*3.9*	*4.5*	*1.5*	*1.4*	*3.6*	*8.5*	*7.8*	*3.2*	*3*	*2.6*	*2.6*	*2.4*
11	0.4	364	28.8	*2.7*	*2.9*	*1.5*	*1.0*	13.4	*10.1*	*5.7*	16.1	*2.1*	*3.3*	*2.3*	*2.2*
12	0.3	452	*15.8*	*8.7*	*4.5*	*1.7*	*1.7*	*5.4*	*7.1*	*10.5*	13.0	*2.7*	*3.3*	*4.1*	*2.0*
13	0.2	339	*15.4*	10.6	*2.9*	*1.8*	*1.7*	*11.1*	*4.9*	12.2	16.5	*0.6*	5.6	*0.3*	*4.6*
14	0.5	407	29.8	*5.4*	*5.1*	*3.9*	3.6	*7.8*	*13.2*	13.8	*14.2*	*5.1*	*1*	*3.4*	9.0
15	0.3	370	*18.3*	*2.8*	*2.6*	*1.7*	*1.1*	*0.8*	*1.0*	13.5	*5.3*	*1.3*	*2.8*	*3.3*	*1.5*
16	0.5	609	*13.5*	16.1	*2.2*	*0.7*	*0.3*	*8.8*	17.1	*3.6*	20.3	*4.0*	*1.2*	*3.9*	*3.0*
CL			23.750	9.890	7.127	4.026	3.001	12.443	13.325	10.681	15.853	5.130	4.745	5.164	6.290

The mfPhNR RAD values were obtained from five concentric annular rings centered on the fovea (R1, central circular area with a radius of 5°; R2, annular areas enclosed between 5° and10°; R3, annular area enclosed between 10° and15°; R4, annular area enclosed between 15° and 20°; R5, annular area enclosed between 20° and 25°) and from eight sectors based on ETDRS sectors: four sectors (S, N, I, T) enclosed between 5° and 10° (R2) and four sectors (S, N, I, T) enclosed between 10° and 20° (R3+R4). The 95% confidence limits (CLs) were derived from controls. *Italics* indicate ERM eyes with abnormal mfPhNR RAD values (reduced from the lower 95% CL limit).

Investigative Ophthalmology & Visual Science

Table 2. Individual Values of mfERG Responses Detected in Eyes With ERMs

	Rings mfERG RAD (nV/deg^2)					ETDRS Sectors mfERG R2 RAD (nV/deg^2)				ETDRS Sectors mfERG R3+R4 RAD (nV/deg^2)			
ERM	**R1**	**R2**	**R3**	**R4**	**R5**	**S**	**N**	**I**	**T**	**S**	**N**	**I**	**T**
1	*44.6*	19.8	*8.2*	*7.7*	*5.7*	*12.1*	*19.5*	22.4	*17.9*	*7.7*	*7.6*	*7.8*	*7.4*
2	*44.8*	*18.6*	*11.5*	8.7	*6.0*	21.3	29.7	24.8	31.8	10.5	10.1	*7.7*	*8.7*
3	49.1	*17.6*	*8.4*	*6.7*	*5.9*	9.9	*21.5*	23.6	25.2	*7.9*	*5.9*	*6.1*	*8.3*
4	*38.9*	*16.8*	11.8	*7.1*	8.0	23.8	*22.4*	23.0	*16.4*	*8.8*	*7.9*	7.7	10.8
5	*28.9*	*18.2*	16.7	10.8	9.7	24.5	*23.0*	*20.7*	27.1	12.1	13.2	13.1	12.9
6	*28.3*	*12.6*	15.9	13.0	9.0	33.0	26.8	*18.1*	26.9	14.1	16.8	10.2	16.0
7	*26.1*	*8.3*	*4.4*	*4.6*	*4.9*	*14.4*	25.9	22.6	*16.1*	*4.7*	*6.5*	*2.7*	9.6
8	*40.8*	*18.5*	*9.7*	*7.5*	*5.9*	21.5	*22.8*	21.8	*19.5*	*8.4*	*8.1*	10.3	*6.3*
9	*34.6*	*15.4*	*8.6*	10.2	*4.8*	26.7	40.7	*20.8*	25.7	*7.3*	13.0	12.5	*6.9*
10	*32.1*	*12.5*	*8.4*	*7.4*	*5.6*	*12.8*	*22.4*	*19.6*	*16.8*	*8.6*	*6.9*	*8.1*	*8.1*
11	*34.6*	*17.8*	*11.0*	*7.8*	*6.0*	19.9	*21.8*	*18.9*	25.8	*8.7*	*7.4*	*8.7*	10.1
12	*27.8*	*16.3*	14.5	8.7	7.5	20.9	29.7	*19.5*	*20.6*	13.0	9.6	9.5	10.5
13	*26.6*	*10.5*	*9.2*	*6.3*	7.2	*12.7*	*21.2*	*18.6*	*19.9*	*6.0*	*6.1*	*7.4*	*8.1*
14	*20.3*	*13.7*	*11.4*	*5.9*	*6.0*	*15.3*	*16.7*	*19.9*	27.4	*7.7*	*6.5*	*9.3*	*8.0*
15	*16.8*	*10.5*	*10*	*8.1*	*5.5*	*15.1*	*19.8*	*19.3*	*20.4*	*8.7*	*8.1*	*8.7*	9.9
16	*17.2*	*8.2*	13.6	9.7	8.7	21.8	26.5	28.5	22.4	10.5	11.0	11.3	10.3
CL	46.400	19.375	11.522	8.317	6.989	19.295	24.365	21.405	20.661	9.466	8.935	9.391	9.516

The mfERG RAD values were obtained from five concentric annular rings centered on the fovea (R1–R5) and from eight sectors based on ETDRS sectors: four sectors (S, N, I, T) enclosed between 5° and 10° (R2) and four sectors (S, N, I, T) enclosed between 10° and 20° (R3+R4). The 95% confidence limits (CLs) were derived from controls. *Italics* indicate ERM eyes with abnormal mfERG RAD values (reduced from the lower 95% CL limit).

Table 3. Means and SDs for mfPhNR RADs Detected in Control and ERM Eyes

				ANOVA, Control Vs. ERM, $f(1, 43)$			
RADs (nV/deg^2)	**Group**	**Mean**	**SD**	***f***	***P***	**Abnormal,* *n***	**Abnormal,* %**
A. mfPhNR ring analysis							
R1	Control	26.576	6.757	—	—	—	—
	ERM	19.613	7.621	9.85	0.003	10	62.50
R2	Control	10.896	3.523	—	—	—	—
	ERM	6.000	4.102	17.45	<0.001	13	81.25
R3	Control	7.848	2.135	—	—	—	—
	ERM	3.306	1.300	59.44	<0.001	16	100
R4	Control	4.296	1.123	—	—	—	—
	ERM	1.563	0.954	66.96	<0.001	16	100
R5	Control	3.683	0.887	—	—	—	—
	ERM	1.313	0.872	73.57	<0.001	15	93.75
B. mfPhNR ETDRS sector analysis							
R2 S	Control	14.393	5.029	—	—	—	—
	ERM	8.913	5.952	10.58	0.002	12	75.00
R2 N	Control	15.593	5.849	—	—	—	—
	ERM	8.763	5.451	14.57	<0.001	13	81.25
R2 I	Control	12.693	5.189	—	—	—	—
	ERM	8.488	3.171	8.61	0.005	13	81.25
R2 T	Control	17.789	4.995	—	—	—	—
	ERM	10.888	6.110	16.51	<0.001	11	68.75
R3+R4 S	Control	5.857	1.875	—	—	—	—
	ERM	2.600	1.537	34.80	<0.001	16	100
R3+R4 N	Control	5.254	1.312	—	—	—	—
	ERM	3.700	1.970	9.86	0.003	12	75.00
R3+R4 I	Control	5.825	1.705	—	—	—	—
	ERM	2.938	1.644	29.94	<0.001	14	87.50
R3+R4 T	Control	7.050	1.960	—	—	—	—
	ERM	3.294	2.580	29.64	<0.001	14	87.50

RAD values were obtained from five concentric annular rings centered on the fovea (R1–R5) in A and from eight sectors based on ETDRS sectors: four sectors (S, N, I, T) enclosed between 5° and 10° (R2) and four sectors (S, N, I, T) enclosed between 10° and 20° (R3+R4) in B.

* The abnormal columns represent the number and percentage of ERM eyes with abnormal mfPhNR RAD values (values lower than the confidence limit).

Investigative Ophthalmology & Visual Science

Table 4. mfPhNR and mfERG Values Yielded by Ring Analysis in the Control and ERM Groups Analyzed by the Segmented Regression Model with Breakpoint Estimation

	Ring 1 + Ring 2 Slope	Ring 3 + Ring 4 + Ring 5 Slope
mfPhNR		
Control eyes	−15.3070 (95% CI, −17.3380 to −13.277)	−2.1232 (95% CI, −3.1384 to −1.108)
ERM eyes	−13.61300 (95% CI, −16.3870 to −10.8380)	−0.99688 (95% CI, −2.3842 to 0.39049)
Difference	−1.694	−1.12632
mfERG		
Control eyes	−30.5070 (95% CI, −33.9270 to −27.08700)	−2.5179 (95% CI, −4.2279 to −0.80777)
ERM eyes	−17.2630 (95% CI, −20.803 to −13.72200)	−2.0906 (95% CI, −3.861 to −0.32023)
Difference	−13.244	−0.4273

CI, confidence interval.

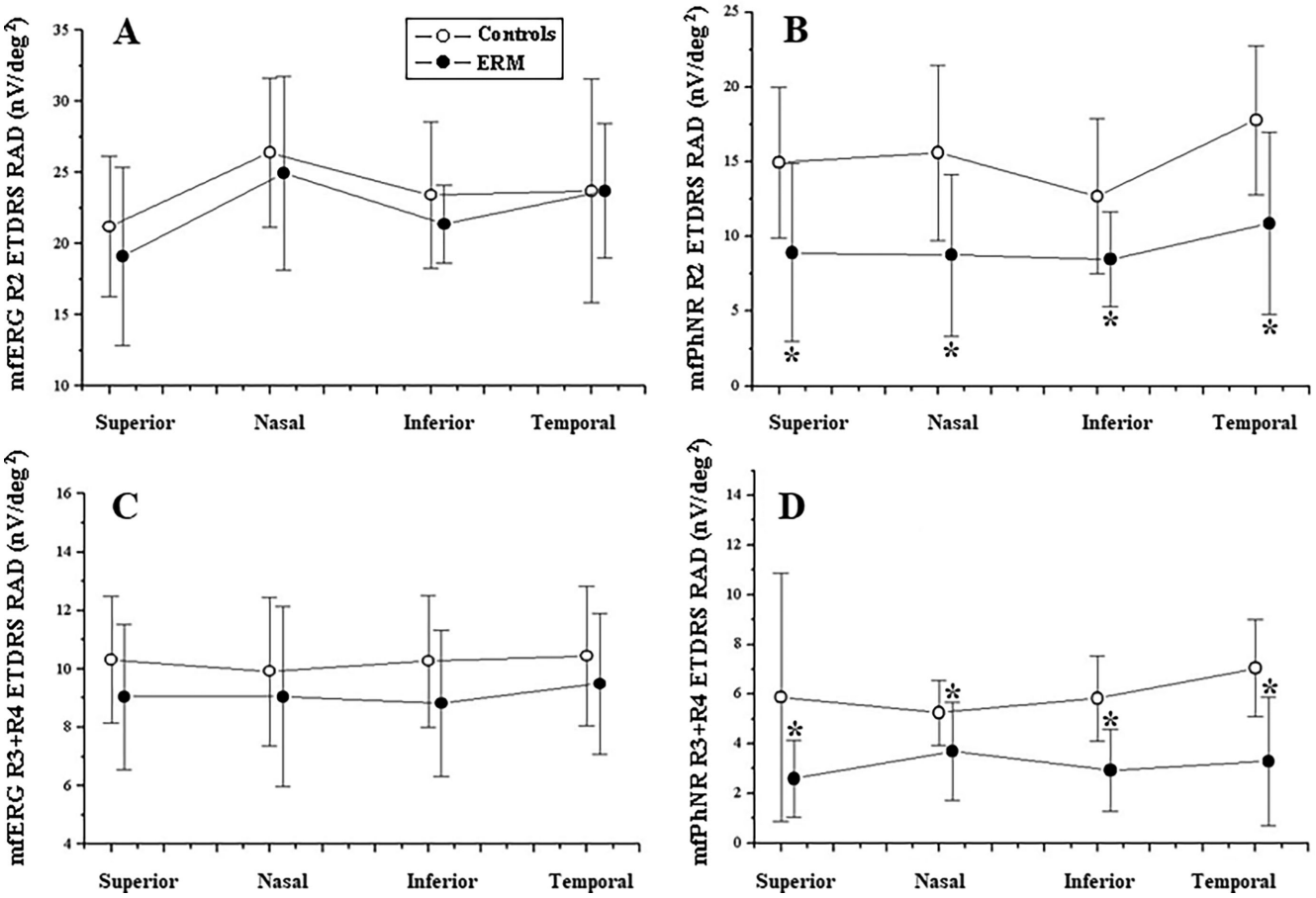

Figure 5. Analysis of mfERG and mfPhNR RADs using ETDRS maps: four sectors (S, N, I, T) between the control and ERM groups. (**A**, **C**) Mean values and 1 SD (*vertical bars*) of mfERG detected between 5° and 10° (R2 S, N, I, T) and 10° and 20° (R3+R4 S, N, I, T). When comparing the ERM data regarding mfERG results to those of the controls, no significant ($P > 0.01$) differences were found between the groups, as reported in Table 5B. (**B**, **D**) Mean values and 1 SD (*vertical bars*) of mfPhNR detected between 5° and 10° (R2 S, N, I, T) and 10° and 20° (R3+R4 S, N, I, T). When the data for the ERM mfPhNR results were compared to those of the controls, significant ($P < 0.01$) differences were found between groups as reported in Table 3B and indicated by an *asterisk*.

from 68.75% in the R2 temporal (T) sector to 100% in the R3+R4 superior (S) sector (Tables 1, 3). On average, considering mfPhNR sector responses detected at 5° to 10° in the R2 S, nasal (N), inferior (I), and T sectors and 10° to 20° in the R3+R4 S, N, I, and T sectors, statistically significant reduced values ($P < 0.01$) were observed in the ERM group compared to the control group. The mean values and the relative statistical analysis between the control and ERM groups are reported in Table 3 and Figures 5B, 5D.

MfERG Responses: Ring Analysis

Considering individual values, reduced mfERG responses were detected in most of the eyes of the ERM group (from 62.50% in R4 and R5 to 93.75% in R1 and R2) (see Tables 2, 5). On average, the mfERG ring responses observed in the ERM group were significantly ($P < 0.01$) reduced exclusively in the central 0° to 10° (R1 and R2), whereas in the more eccentric concentrical areas between

Table 5. Mean Values and SDs for mfERG RADs Detected in Control and ERM Eyes

RAD (nV/deg^2)	Group	Mean	SD	ANOVA, Control Vs. ERM, $f(1, 43)$ f	ANOVA, Control Vs. ERM, $f(1, 43)$ P	Abnormal,* n	Abnormal,* %
A. mfERG ring analysis							
R1	Control	51.557	13.299	—	—	—	—
	ERM	31.969	9.816	26.38	0.003	15	93.75
R2	Control	21.050	4.320	—	—	—	—
	ERM	14.367	3.727	26.82	<0.001	15	93.75
R3	Control	12.643	2.890	—	—	—	—
	ERM	10.831	3.191	3.71	0.061	11	68.75
R4	Control	9.068	1.936	—	—	—	—
	ERM	8.138	0.954	2.25	0.141	10	62.50
R5	Control	8.138	2.055	—	—	—	—
	ERM	6.650	1.507	3.81	0.057	10	62.50
B. mfERG ETDRS sector analysis							
R2 S	Control	21.207	4.932	—	—	—	—
	ERM	19.106	6.276	1.51	0.226	7	43.75
R2 N	Control	26.404	5.258	—	—	—	—
	ERM	24.593	5.780	1.10	0.300	10	62.50
R2 I	Control	23.411	5.171	—	—	—	—
	ERM	21.381	2.724	2.11	0.153	9	56.25
R2 T	Control	23.714	7.875	—	—	—	—
	ERM	22.494	4.726	0.32	0.578	8	50
R3+R4 S	Control	10.307	2.169	—	—	—	—
	ERM	9.044	2.474	3.07	0.087	11	68.75
R3+R4 N	Control	9.921	2.543	—	—	—	—
	ERM	9.044	3.080	1.04	0.314	10	62.50
R3+R4 I	Control	10.264	2.253	—	—	—	—
	ERM	8.819	2.500	3.91	0.055	10	62.50
R3+R4 T	Control	10.443	2.392	—	—	—	—
	ERM	9.494	2.413	1.58	0.215	8	50.00

RAD values were obtained from five concentric annular rings centered on the fovea (R1–R5) in A and from eight sectors based on ETDRS sectors: four sectors (S, N, I, T) enclosed between 5° and 10° (R2) and four sectors (S, N, I, T) enclosed between 10° and 20° (R3+R4) in B.
* The abnormal columns represent the number and percentage of ERM eyes with abnormal mfERG RAD values (values lower than the confidence limit).

central 10° and 25° (R3, R4, and R5) no statistically significant ($P > 0.01$) differences between the control and ERM groups were found. The mean values and relative statistical analyses between groups are reported in Table 5.

When analyzing mfERG values by segmented regression model with breakpoint estimation in the control and ERM groups, the difference slope between R1 and R2 and R3 to R5 was not constant (−13.244 vs. −0.4273); it was greater in the first two rings than in R3 to R5, indicating that in the central 0° to 10° there was greater outer retinal dysfunction than in the 10° to 25° eccentricity in the ERM group. This is shown in Figure 4B and Table 4.

MfERG Responses: ETDRS Sector Analysis

Considering individual values, reduced mfERG sector responses on variable percentages of ERM eyes (from 43.75% in R2 S to 68.75% in R3+R4 S) were detected (see Tables 2, 5). On average, considering the mfERG sector responses detected in both 5° to 10° (R2 S, N, I, T) and in 10° to 20° (R3+R4 S, N, I, T) no statistically significant ($P > 0.01$) differences between the control and ERM groups were found. The mean values and relative statistical analyses between the control and ERM groups are shown in Table 5 and Figures 5A and 5C.

Correlations Among mfPhNR and mfERG Responses, BCVA, and CRT Values

As shown in Figures 6A and 6B, when plotting mfERG ring RAD values detected in 0° to 5° and in the central 5° to 10° (R1 and R2) against the corresponding mfPhNR values, no statistically significant ($P > 0.01$) linear correlation was found in the ERM group. In ERM eyes, the reduced BCVA correlated linearly ($P < 0.01$) to the reduced mfERG R1 responses, whereas there was no correlation between BCVA and mfPhNR R1 responses (see Figure 6C and 6D). MfERG and mfPhNR R1 responses did not correlate with CRT (Figure 6E and 6F) in ERM eyes.

Discussion

The aim of our work was to evaluate, in ERM eyes, the function of macular ganglion cells and nerve fibers (by mfPhNR recordings) and of macular photoreceptors and bipolar cells (by mfERG recordings), as well as to study the correlation between the functions of these different retinal elements with changes in BCVA and CRT. The novelty of this work is that, although pioneering electrophysiological studies have assessed an inner retinal dysfunction in ERM eyes located in the central 9° (by focal PERG responses),[14] actually it is possible to detect functional impairment of the inner reti-

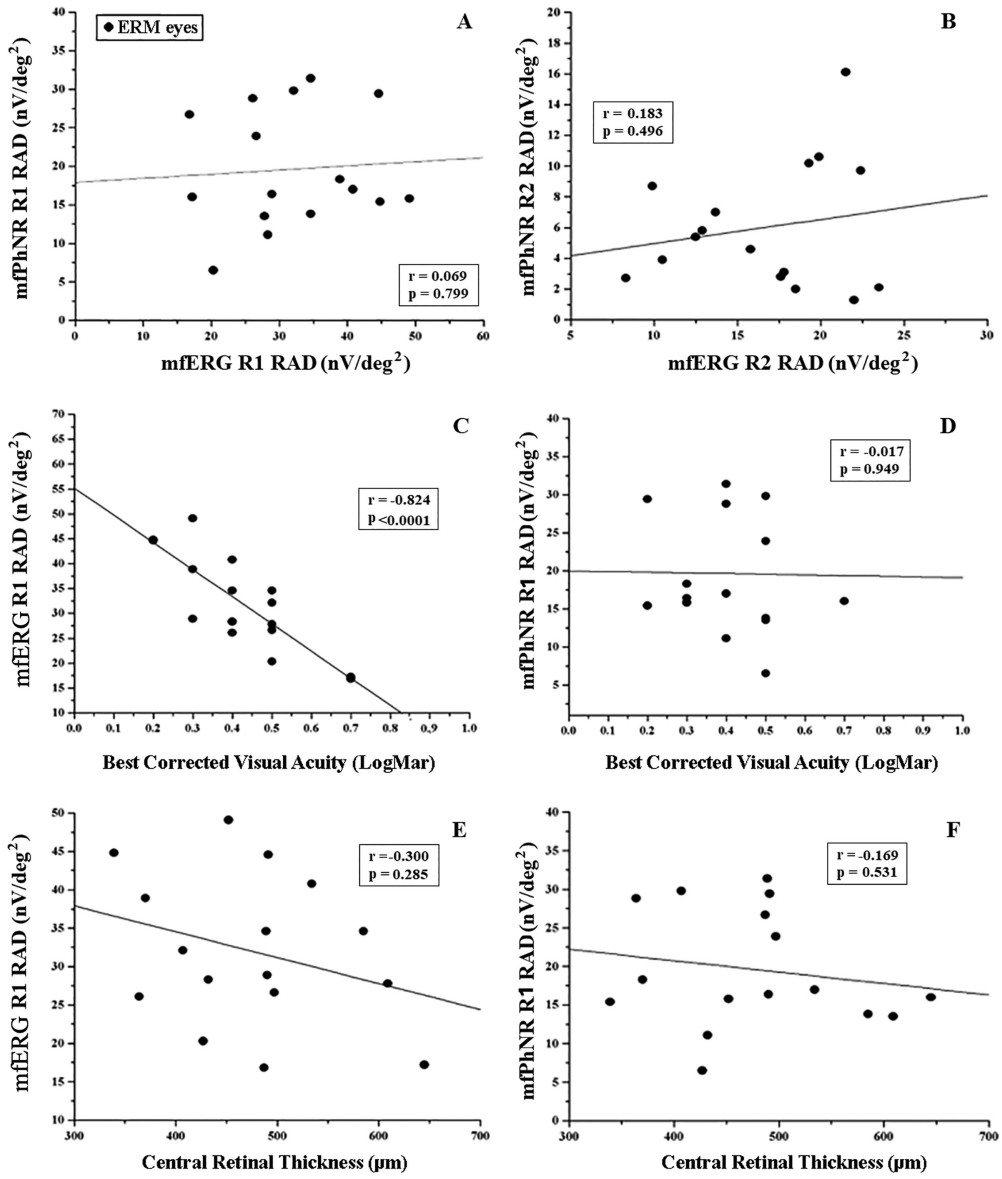

Figure 6. (**A**, **B**) Linear plots between mfPhNR and mfERG RADs from the central retinal area (R1) and in the annular areas enclosed between 5° and 10° (R2) in eyes with ERMs. (**C**, **D**) Correlation between the BCVA (logMAR) values and RADs detected from the central retinal area (R1) by mfERG and mfPhNR, respectively. (**E**, **F**) Relationship between central retinal thickness (µm) and RADs detected in the central retinal area (R1) by mfERGs and mfPhNRs, respectively.

nal elements located in different macular circular areas with different eccentricity from the fovea (ring analysis) or in different macular sectors (sector analysis) by the innovative mfPhNR technique.[17,29]

In our ERM eyes, a significant reduction of mfPhNR RADs was observed in all rings and sectors, suggesting that a dysfunction of the retinal ganglionic elements cannot be exclusively detected in the more central 10° (R1 and R2) but that it extends until the 25°of the foveal eccentricity (R3, R4, and R5); in addition, the observed dysfunction was constant from the fovea up to the retinal periphery. This finding can be ascribed to the peculiar macular and extramacular morphological changes occurring in the enrolled stage 4 ERM eyes. It is well known that this stage is characterized by significant retinal thickening, remarkable anatomic macular disruption, and ectopic inner foveal layers (EIFLs). Thus, it is likely that all of these inner retinal structural changes could induce a wide and diffuse inner retinal dysfunction, involving mainly retinal ganglion cells (RGCs), which are closer to the ERMs. This is in keeping with the results by Shin et al.,[30] indicating that the RGC layer is the retinal layer primarily affected by ERMs.[30] In the same work, it was suggested that the involvement of pre-ganglionic elements can occur during the ERM evolution.[30]

In our study, the function of localized macular preganglionic elements (photoreceptors and bipolar cells) was studied by assessing mfERG recordings and using two different topographies. In our ERM cohort, mfERG recordings showed significantly reduced RAD exclusively in R1 and R2, whereas no statically significant differences were found between the ERM and control groups in the more peripheral rings (R3, R4, and R5 RADs). This finding suggests that, in

our ERM eyes, a dysfunction of outer retinal layers occurs in the more central retinal areas (central 0° to 10°) with possible functional sparing of the same retinal elements located in the more peripheral macular areas (within 10° and 25°). This finding was supported when the segmented regression models with breakpoint estimation showed a great difference of slope only in the central 0° to 10°. Our findings are consistent with previously published results, indicating a pre-ganglionic dysfunction exclusively in the more central macular areas.[31,32]

The mfERG analysis of the macular ETDRS sectors in which the function of the more central macular area (R1) was excluded showed no statistically significant differences in RAD values between the control and ERM groups. This can be explained by previously mentioned data, suggesting that, in ERM eyes, there is normal function in the pre-ganglionic elements located over the central 10°. Alternatively, it might be possible that the ring analysis could have masked some impairment occurring in one or more sectors; however, this possibility can be excluded by the results obtained by the sector analysis.

The observed central pre-ganglionic dysfunction may be ascribed to two possible factors: (1) displacement that the ERMs, endowed with contractile capability, apply on the outer retinal layers[33,34] and (2) retrograde transneuronal degeneration and/or impaired axonal transport.[35] In fact, based on recent acquisitions, ERMs that tightly adhere to the surface of the ILM not only affect the entire retinal structure (as evidenced by increased CRT), but also induce a displacement along both the sagittal and coronal planes.[33] ERMs causes inward traction at the foveal pit, which is reflected at the interface between the inner and outer segments, without severely damaging the photoreceptor cell bodies themselves,[35] although reducing their function.

The tangential traction forces of ERMs pull the underlying inner foveal layers, from the Henle fiber layer to the outer nuclear layer (ONL), toward the foveal center, resulting in disappearance of the foveal pit. The displacement, induced by the presence of ERM, could change the synaptic connections between the inner and outer retinal elements. From our results, this steadily involves the inner retina from the foveal center up to the periphery.

On the other hand, inner nuclear layer (INL) damage due to ERM-induced neuronal kinking may initiate potential retrograde neuronal degeneration.[35] Commonly, the ONL, which contains photoreceptor bodies (presynaptic elements), delivers visual input to the elements of the INL (bipolar postsynaptic elements) and to RGCs. If the RGCs are primarily damaged, synaptic connections with the outer retina are stretched and lost and thus are not able to receive the visual impulse from the photoreceptors, causing loss of trophic support of the target (RGCs).

It is interesting that, in our ERM eyes, the dysfunctions occurring in macular elements of outer and inner retinal layers located in the more central macular areas (detected by reduced R1 and R2 mfERGs and mfPhNR RADs, respectively) were not linearly correlated. Apart from the above-mentioned unbalanced synaptic connection between photoreceptors and bipolar cells and RGCs, other factors may explain the lack of correlation. In this context, a key role in the retinal layered structure is played by Müller cells and glial cells, which span almost the entire thickness of the retina and are primarily responsible for mechanical force transmission to photoreceptors.[36,37] Throughout their path, Müller cells attenuate mechanical stresses and increase compliance of the retina; nevertheless, they may interact with other cellular elements by changing their connections[37] (see below). In addition, due to the wide known structural displacement of the retinal planes.[33] Another hypothesis is that the presynaptic and the postsynaptic elements might become rewired through non-conventional neuronal pathways. This suggestion is supported by the knowledge that, in the presence of tractional forces from the ERMs, gliosis processes, including upregulation of glial intermediate filaments such as vimentin and glial fibrillary acidic protein (GFAP), are triggered by increasing tissue stiffness, causing the loss of physiological connections between the inner and outer retina. Wang et al.[38] studied the crucial role of glial cells and reported that a high density of glial cells resulted in morphological changes such as outer retinal inward projection and inner retinal thickening on SD-OCT images. They also found that a high glial cell density was associated with poor BCVA after surgery.[38]

Secondary aims of our work were to correlate the outer and inner macular dysfunction with BCVA and CRT values. The BCVA reduction observed in ERM eyes correlated only with the outer retinal dysfunction (reduced R1 mfERG RADs) and not with the inner retinal impairment (reduced R1 mfPhNR RADs). This result is consistent with previous studies[36–40] that have found that visual dysfunction in ERM patients is caused by the traction of photoreceptor cells by Müller cells[37] and by the observed loss of the regularity of the spatial arrangement of the cone mosaic detected by adaptive optics scanning laser ophthalmoscopy.[39] The integrity of the ellipsoid zone and the external limiting membrane, which reflects the continuity of the structural and metabolic support between photoreceptors and Müller cells, is primarily responsible for BCVA status.[36,37] Thus, our findings of significant linear correlation between mfERG R1 RADs and BCVA in the ERM group confirm the previous evidence.[36–40]

Conversely, an absence of linear correlation between mfPhNR foveal (R1) RADs and BCVA in our cohort of stage 4 ERM eyes was observed. Similar studies performed using mfPhNR in ERMs have not been reported, so our results cannot be confirmed by previously described data. Nevertheless, a linear correlation between inner retinal dysfunction (assessed by focal PERG responses) and reduced BCVA has been reported[14]; however, in that work the stage of ERM was not considered, and the inner retinal dysfunction was observed in a central retinal area (central 9°) larger than the central 0° to 5° area from which the mfPhNR R1 reduced RADs were derived.

With regard to this lack of correlation, because the observed outer and inner macular dysfunctions were not related (only dysfunction of the central outer retina was correlated to the BCVA reduction), we can only hypothesize that, in ERM eyes, impaired synaptic signaling and neuronal intraretinal transmission could occur with consequent functional inner/outer retina decoupling. Thus, the reduced BCVA we observed was not dependent on central inner retina (0°–5°) dysfunction as suggested by the above-mentioned decoupling.

When considering the relationship between CRT and R1 mfERG and mfPhNR RADs, no correlation was found in the ERM group, thus indicating a morphofunctional dissociation and suggesting that different structural factors, such as the presence of EIFLs, integrity of the INL, inner segment/outer segment junctions, and photoreceptor outer segment length, and the presence of disorganization of reti-

Investigative Ophthalmology & Visual Science

nal inner layers,[41–45] might be better indicators of morpho-functional associations. In addition, the absence of a relationship between morphological and functional indicators could be due to the fact that CRT describes full retinal thickness changes without distinguishing the isolated contribution of outer and inner retinal layers to ERM pathophysiology.

In conclusion, in ERM stage 4 eyes, an unrelated dysfunction of both inner and outer macular layers occurs in the central 0° to 10° and exclusive inner macular dysfunction in the more peripheral areas (10°–25°). The reduction of BCVA depended only on the central outer macular dysfunction. Our results apply exclusively to ERM stage 4, which may be considered a limitation of the study. It would be interesting to explore whether the observed inner and/or outer retinal dysfunction may occur in earlier stages (stages 2 and 3) of ERM to elucidate functional progression dynamics.

Acknowledgments

The authors thank Federica Petrocchi, Elisa Tronti, Giuliana Facciolo, and Francesca Petruzzella for executing the visual psychophysical assessments and Maria Luisa Alessi for technical assistance in electrophysiology and figure presentation.

Supported partially by the Italian Ministry of Health and Fondazione Roma.

Disclosure: **V. Parisi**, None; **L. Ziccardi**, None; **C. Dell'Aquila**, None; **L. Barbano**, None; **M. D'Andrea**, None; **S. Giammaria**, None; **G. Ripandelli**, None; **L. Placentino**, None; **R. dell'Omo**, None; **T. Rossi**, None

References

1. Fung AT, Galvin J, Tran T. Epiretinal membrane: a review. *Clin Exp Ophthalmol*. 2021;49(3):289–308.
2. Romano MR, Cennamo G, Amoroso F, et al. Intraretinal changes in the presence of epiretinal traction. *Graefes Arch Clin Exp Ophthalmol*. 2017;255(1):31–38.
3. da Silva RA, Roda VMP, Matsuda M, et al. Cellular components of the idiopathic epiretinal membrane. *Graefes Arch Clin Exp Ophthalmol*. 2022;260(5):1435–1444.
4. Yang X, Wang Z, Yu Y, et al. Changes of fixation stability and location after epiretinal membrane surgery. *Retina*. 2022;42(5):883–891.
5. Cacciamani A, Cosimi P, Di Nicola M, Di Martino G, Ripandelli G, Scarinci F. Correlation between outer retinal thickening and retinal function impairment in patients with idiopathic epiretinal membranes. *Retina*. 2019;39(2):331–338.
6. Ripandelli G, Scarinci F, Piaggi P, et al. Macular pucker: to peel or not to peel the internal limiting membrane? A microperimetric response. *Retina*. 2015;35(3):498–507.
7. Wilkins JR, Puliafito CA, Hee MR, et al. Characterization of epiretinal membranes using optical coherence tomography. *Ophthalmology*. 1996;103(12):2142–2151.
8. Lubiński W, Gosławski W, Krzystolik K, Mularczyk M, Kuprjanowicz L, Post M. Assessment of macular function, structure and predictive value of pattern electroretinogram parameters for postoperative visual acuity in patients with idiopathic epimacular membrane. *Doc Ophthalmol*. 2016;133(1):21–30.
9. Gelormini F, Ricardi F, Parisi G, et al. Visual performance and predictive OCT biomarkers in epiretinal membrane assessment: beyond distance visual acuity. *Invest Ophthalmol Vis Sci*. 2025;66(1):31.
10. Massin P, Allouch C, Haouchine B, et al. Optical coherence tomography of idiopathic macular epiretinal membranes before and after surgery. *Am J Ophthalmol*. 2000;130(6):732–739.
11. Govetto A, Lalane RA, 3rd, Sarraf D, Figueroa MS, Hubschman JP. Insights into epiretinal membranes: presence of ectopic inner foveal layers and a new optical coherence tomography staging scheme. *Am J Ophthalmol*. 2017;175:99–113.
12. Parisi V, Falsini B. Electrophysiological evaluation of the macular cone system: focal electroretinography and visual evoked potentials after photostress. *Semin Ophthalmol*. 1998;13(4):178–188.
13. Hood DC. Assessing retinal function with the multifocal technique. *Prog Retin Eye Res*. 2000;19(5):607–646.
14. Parisi V, Coppè AM, Gallinaro G, Stirpe M. Assessment of macular function by focal electroretinogram and pattern electroretinogram before and after epimacular membrane surgery. *Retina*. 2007;27(3):312–320.
15. Tanikawa A, Horiguchi M, Kondo M, Suzuki S, Terasaki H, Miyake Y. Abnormal focal macular electroretinograms in eyes with idiopathic epimacular membrane. *Am J Ophthalmol*. 1999;127(5):559–564.
16. Moschos M, Apostolopoulos M, Ladas J, et al. Assessment of macular function by multifocal electroretinogram before and after epimacular membrane surgery. *Retina*. 2001;21(6):590–595.
17. Barbano L, Ziccardi L, Antonelli G, et al. Multifocal electroretinogram photopic negative response: a reliable paradigm to detect localized retinal ganglion cells' impairment in retrobulbar optic neuritis due to multiple sclerosis as a model of retinal neurodegeneration. *Diagnostics (Basel)*. 2022;12(5):1156.
18. Parisi V, Barbano L, Antonelli G, et al. Topographical correlation between structural and functional impairment of the macular inner retinal layers in multiple sclerosis eyes with a history of optic neuropathy. *J Clin Med*. 2023;12(22):7175.
19. Parisi V, Ziccardi L, Giammaria S, et al. Dysfunction and morphological involvement of inner macular layers in glaucoma. *J Clin Med*. 2024;13(22):6882.
20. Falsini B, Fadda A, Iarossi G, et al. Retinal sensitivity to flicker modulation: reduced by early age-related maculopathy. *Invest Ophthalmol Vis Sci*. 2000;41(6):1498–1506.
21. Varano M, Parisi V, Tedeschi M, et al. Macular function after PDT in myopic maculopathy: psychophysical and electrophysiological evaluation. *Invest Ophthalmol Vis Sci*. 2005;46(4):1453–1462.
22. Falsini B, Bardocci A, Porciatti V, Bolzani R, Piccardi M. Macular dysfunction in multiple sclerosis revealed by steady-state flicker and pattern ERGs. *Electroencephalogr Clin Neurophysiol*. 1992;82(1):53–59.
23. Parisi V, Ziccardi L, Centofanti M, et al. Macular function in eyes with open-angle glaucoma evaluated by multifocal electroretinogram. *Invest Ophthalmol Vis Sci*. 2012;53(11):6973–6980.
24. Parravano M, Fragiotta S, Costanzo E, et al. Metabolic, microvascular, and structural predictors of long-term functional changes evaluated by multifocal electroretinogram in type 1 diabetes. *Biomedicines*. 2024;12(11):2614.
25. Barbano L, Ziccardi L, Landi D, et al. Assessment of macular function by multifocal electroretinogram in patients with multiple sclerosis treated with fingolimod. *Adv Ther*. 2021;38(7):3986–3996.
26. Ziccardi L, Barbano L, Boffa L, et al. Functional assessment of outer and middle macular layers in multiple sclerosis. *J Clin Med*. 2020;9(11):3766.
27. Sperduto RD, Clemons TE, Lindblad AS, Ferris FL, 3rd, Age-Related Eye Disease Study Research Group. Cataract classification using serial examinations in the age-related eye

disease study: Age-Related Eye Disease Study Report No. 24. *Am J Ophthalmol*. 2008;145(3):504–518

28. Hood DC, Bach M, Brigell M, et al. ISCEV standard for clinical multifocal electroretinography (mfERG) (2011 edition). *Doc Ophthalmol*. 2012;124(1):1–13.
29. Frishman L, Sustar M, Kremers J, et al. ISCEV extended protocol for the photopic negative response (PhNR) of the full-field electroretinogram. *Doc Ophthalmol*. 2018;136(3):207–211.
30. Shin MK, Kim SI, Park SW, Byon IS, Kim HW, Lee JE. Evaluation of macular function using pattern electroretinogram in idiopathic epiretinal membrane. *Asia Pac J Ophthalmol (Phila)*. 2015;4(5):267–272.
31. Hosoda Y, Ooto S, Hangai M, Oishi A, Yoshimura N. Foveal photoreceptor deformation as a significant predictor of postoperative visual outcome in idiopathic epiretinal membrane surgery. *Invest Ophthalmol Vis Sci*. 2015;56(11):6387–6393.
32. Lee JW, Park SY, Kim PS, Cho IH, Kim HD. Correlations among metamorphopsia test scores, optical coherence tomography findings and multifocal electroretinogram responses in epiretinal membrane patients. *Doc Ophthalmol*. 2021;142(3):293–304.
33. Rossi T, Querzoli G, Cosimi P, et al. Three-dimensional retinal displacement before and after macular pucker surgery. *Retina*. 2024;44(8):1329–1336.
34. Scarinci F, Querzoli G, Cosimi P, et al. Retinal tectonics after macular pucker surgery: thickness changes and en face displacement recovery. *Retina*. 2024;44(1):102–110.
35. Cho KH, Park SJ, Woo SJ, Park KH. Correlation between inner-retinal changes and outer-retinal damage in patients with idiopathic epiretinal membrane. *Retina*. 2018;38(12):2327–2335.
36. Govetto A, Bhavsar KV, Virgili G, et al. Tractional abnormalities of the central foveal bouquet in epiretinal membranes: clinical spectrum and pathophysiological perspectives. *Am J Ophthalmol*. 2017;184:167–180.
37. Govetto A, Hubschman JP, Sarraf D, et al. The role of Müller cells in tractional macular disorders: an optical coherence tomography study and physical model of mechanical force transmission. *Br J Ophthalmol*. 2020;104(4):466–472.
38. Wang LC, Lo WJ, Huang YY, et al. Correlations between clinical and histopathologic characteristics in idiopathic epiretinal membrane. *Ophthalmology*. 2022;129(12):1421–1428.
39. Ooto S, Hangai M, Takayama K, et al. High-resolution imaging of the photoreceptor layer in epiretinal membrane using adaptive optics scanning laser ophthalmoscopy. *Ophthalmology*. 2011;118(5):873–881.
40. Matos AMF, Defina RLS, Costa-Cunha LVF, et al. Correlation between retinal sensitivity assessed by microperimetry and structural abnormalities on optical coherence tomography after successful epiretinal membrane surgery. *Int J Retina Vitreous*. 2024;10(1):24.
41. Govetto A, Virgili G, Rodriguez FJ, Figueroa MS, Sarraf D, Hubschman JP. Functional and anatomical significance of the ectopic inner foveal layers in eyes with idiopathic epiretinal membranes: surgical results at 12 months. *Retina*. 2019;39(2):347–357.
42. Okamoto F, Sugiura Y, Okamoto Y, Hiraoka T, Oshika T. Inner nuclear layer thickness as a prognostic factor for metamorphopsia after epiretinal membrane surgery. *Retina*. 2015;35(10):2107–2114.
43. Inoue M, Arakawa A, Yamane S, Kadonosono K. Long-term outcome of preoperative disrupted inner/outer segment junctions assessed using spectral-domain optical coherence tomography in patients with idiopathic epiretinal membrane. *Ophthalmologica*. 2012;228(4):222–228.
44. Shiono A, Kogo J, Klose G, et al. Photoreceptor outer segment length: a prognostic factor for idiopathic epiretinal membrane surgery. *Ophthalmology*. 2013;120(4):788–794.
45. Zur D, Iglicki M, Feldinger L, et al. Disorganization of retinal inner layers as a biomarker for idiopathic epiretinal membrane after macular surgery—the DREAM Study. *Am J Ophthalmol*. 2018;196:129–135.